Applications, features, and mechanistic aspects of liquid water beam desorption mass spectrometry

B. Abel [a,b,*], A. Charvat [b], U. Diederichsen [c], M. Faubel [d],
B. Girmann [c], J. Niemeyer [e], A. Zeeck [c]

[a] *Institut für Physikalische Chemie der Universität Göttingen, Tammannstrasse 6, D-37077 Göttingen, Germany*
[b] *Max-Planck-Institut für Biophysikalische Chemie, Am Fassberg 11, D-37077 Göttingen, Germany*
[c] *Institut für Organische und Biomolekulare Chemie der Universität Göttingen, Tammannstrasse 2, D-37077 Göttingen, Germany*
[d] *Max-Planck-Institut für Dynamik und Selbstorganisation, Bunsenstrasse 10, D-37073 Göttingen, Germany*
[e] *Fakultät für Agrarwissenschaften, Institut für Agrikulturchemie, Carl-Sprengel-Weg 1, 37075 Göttingen, Germany*

Abstract

In the present study we highlight recent applications of liquid beam desorption mass spectrometry for the analysis of biomolecules. The protonated macromolecules are desorbed from a 10 μm thick liquid jet in vacuum with an IR laser pulse tuned in resonance with the OH stretch vibration of water. Cytochrome *c*, viscotoxin A3, synthetic analogues of DNA and nucleobase substituted β-peptides (PNA like oligomers), bovine serum albumin (BSA), as well as specifically designed pharmaceutical macromolecules have been investigated. The salt and buffer tolerance has been measured for the desorption of cytochrome *c*. For the PNA oligomers it has been shown that a mixture can be desorbed and that the relative intensity of the mass peaks reflects relative concentrations in solution. With diluted BSA water solutions it has been demonstrated that the desorption technique provides a quantitative measure of BSA in solution. The gas phase signal of singly protonated BSA desorbed from a series of well defined solution concentrations has been found to be linear over at least three orders of magnitude. This feature appears to be promising for quantitative online monitoring applications of this technique. Beyond applications of this technique mechanistic aspects of the poorly characterized desorption mechanism are discussed. With a field-free-drift time-of-flight approach we were able to monitor features of the desorption process by selecting fractions of the broad velocity distribution of desorbed species using an ion optics acting as an ion gate. The observed features were discussed within a "desorption/ionization" model featuring the interplay of an explosive thermal and a shock wave dispersion of the microfilament controlling the ejection of hot nano-droplets and microsolvated molecules as well as their desolvation.
© 2005 Elsevier B.V. All rights reserved.

1. Introduction

In the past 20 years a number of so-called soft ionization methods have been developed and used with success to analyze biomolecules via powerful gas phase mass spectrometry [1–4]. A new and exciting technique to study biomolecules desorbed from their natural environment (water) is laser in-

duced liquid beam desorption mass spectrometry, recently introduced by Brutschy and co-workers [5–11] (LILBID, laser induced liquid beam ionization/desorption); it became feasible after the liquid microwater beam technique in vacuum was developed [12]. In pioneering work of Brutschy and co-workers [5–11] and in recent publications of the Göttingen group [13–15] it was shown that this method has a large potential for the analysis of many macro- and biomolecules.

The experimental approach enables a very soft desorption of protonated or ionic aggregates of supra-molecular species via laser induced desorption with an infrared laser tuned to the OH-stretch vibration of liquid water. A significant ad-

vantage for analytical applications is that with this approach post-desorption ionization with a second laser [16,17] is not necessary which nearly completely avoids fragmentation. Although, several applications of the techniques have now been published – basically by two groups – demonstrating that the technique is able to isolate biomolecules with a laser from "bulk water" in vacuum, the mechanism is far from being adequately understood. This and experimental problems have been the reason why the approach has not matured to a powerful analytical technique yet and has not advanced to a serious competitor for the laser induced solid matrix desorption and electrospray techniques, although, its potential is obviously high. In the present article we summarize applications, show important features and discuss possible mechanism(s) of the process, i.e., answer the question why the technique works at all. Another important aspect of the present study was the question whether liquid beam desorption mass spectrometry provides a quantitative tool for measuring concentrations of biomolecules in solution directly.

2. Experimental approach

The present approach is very straightforward and conceptually simple. We employ a thin water beam (diameter $\sim 10\,\mu m$, flow speed $\sim 40\,m\,s^{-1}$) containing the compounds under investigation which is ejected with high pressure (10–20 bar) into the vacuum chamber (see Fig. 1) [13,14]. Its parameters like temperature, concentration, and pH can be controlled precisely. The liquid jet is rapidly heated within 7 ns in the focus of an IR laser pulse tuned in resonance with the OH-stretch absorption of bulk water at 2.7–2.8 μm. At this wavelength the penetration depth is somewhat smaller than the beam diameter. The absorbed energy of the IR laser in water is redistributed within picoseconds [18,19] and heats up the irradiated volume. The liquid water beam in turn rapidly disintegrates and produces a mixture of hot gas, microdroplets and protonated biomolecules embedded in clusters of various size or nano-droplets with sizes on the order of the biomolecules. The bigger aggregates can be observed in high speed photography of the process (Fig. 1a). A small fraction of the charged (water) aggregates (within a small solid angle) moves in a field-free space to the entrance slit of the mass spectrometer containing the ion optics (Fig. 1b). During this time (a few microseconds) continuous evaporation of water from the aggregates may dissipate heat and in turn stabilize the aggregates and eventually lead to isolated or clustered biomolecules containing a low net charge (e.g., attachment of protons). The pulsed ion optics of the spectrometer is used here for the acceleration of the molecules for further mass analysis and – most importantly – it acts as a gate for the incoming ionic aggregates. Varying the time Δt, i.e., the time between laser pulse and trigger of the ion optics, allows us to monitor different fractions of molecules of the time dependent desorption process. It is interesting to note that details of the time dependent desorption process and
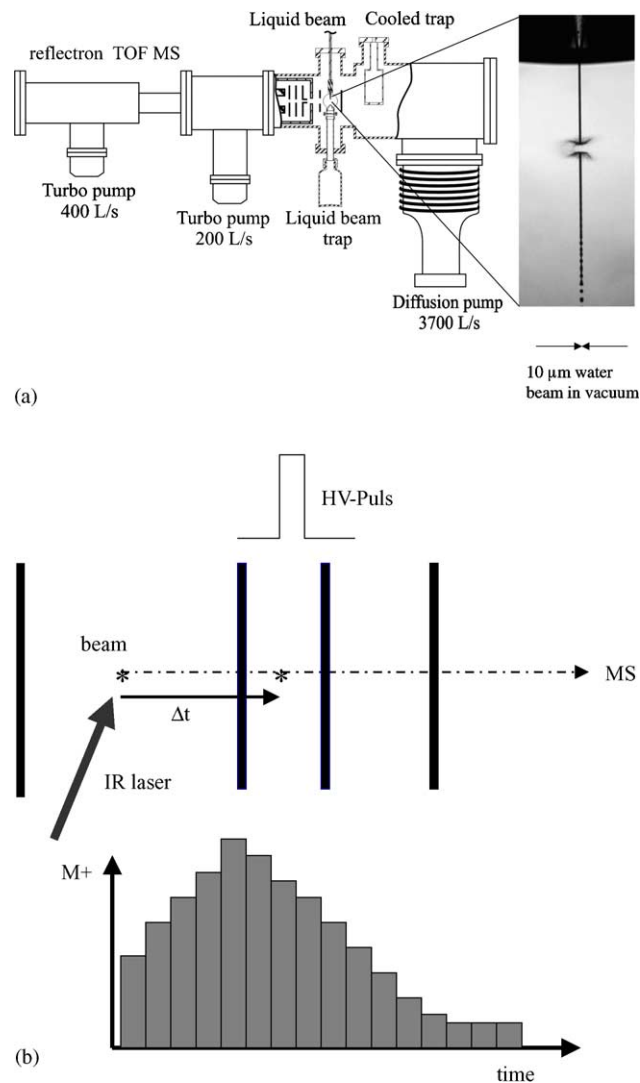
Fig. 1. (a) Vacuum setup containing the liquid beam in vacuum; the time-of-flight mass spectrometer (TOF MS) is used to detect the desorbed ions or ionic aggregates. The right picture displays an enlarged high speed photographic view of the exploding 10 μm liquid water beam in the experiments, $\sim 1\,\mu s$ after heating with a pulsed IR laser tuned to 2650 nm (laser pulse approaching from the right side). (b) Concept of fast laser induced liquid beam desorption of ions and ionic aggregates in a field free drift region and the measurement of sections of the velocity distribution via gated ion optics of the time-of-flight mass spectrometer.

ions/aggregates of different genesis are nicely projected onto the drift times Δt in the field free region (Fig. 1b).

A detailed description of our experimental apparatus is given elsewhere [14]. Thus, only a brief summary is given here. A HLPC pump (Gynkotek, Model 300C) is used to inject the liquid water at 10 bar through a convergent quartz nozzle with diameter of 14 μm into the main vacuum chamber at a flow rate of 0.3 ml min^{-1}. Two centimeter beyond the nozzle the liquid beam could be trapped in a novel liquid water beam trap described elsewhere [13,14]. A cryopump and an oil diffusion pump backed up by a Roots blower and primary pumps held the working pressure at 5×10^{-5} mbar. Tunable nanosecond infrared radiation at a

repetition rate of 20 Hz in the energy range between 0.4 and 0.8 mJ pulse^{-1} was generated with a difference frequency generator (Inrad, Autotracker III). The wavelength was tuned at the blue side of the OH bulk absorption band of water in the range 2550–2850 nm. The IR beam was expanded and tightly focused onto the liquid beam reaching an intensity of about 10^8 W cm^{-2} in the focal plane. The size of the focus ($d = 50$ μm as measured with a knife edge technique) was still significantly larger than the water filament size (by purpose in order to avoid plasma formation). A 1.5 mm diameter skimmer (Beam Dynamics) placed at a distance of 10 mm in the direction perpendicular to both the liquid and the laser beam forms the entrance aperture of a reflectron time-of-flight (re-TOF) mass spectrometer (Kaesdorf, Type RTF10) equipped with a large area (40 mm diameter) microchannel plate detector (Burle, 10 μm pore size). Only positive ions could be detected with the current electronics. In the present setup no ion optics is used for steering and manipulating the ions in front of the mass spectrometer. The repeller and extraction electrodes of the mass spectrometer are switched to high potential (typically 3–6 kV) after a variable delay time Δt allowing for the acceleration and subsequent mass analysis of the charged species that just reached the acceleration region of the mass spectrometer. In front of the detector the ions were post-accelerated to 10 kV in order to improve the detection efficiency. Time-of-flight spectra were recorded after amplification with a 150 MHz (500M samples/s) 8 bit digitizer card (Acquiris, Model DP105) and further processed and stored in a computer. For mass calibration of the time-of-flight traces in the low mass region (<1000 Da) protonated multimers of arginine (up to the octamer) and in the high mass region mass standards such as insulin, myoglobin, lysozyme were used.

Biomolecules used in the experiments were obtained from different commercial and non-commercial sources. Cytochrome *c* from horse heart muscle and bovine serum albumin was purchased from Acros Organics (90% purity). Amino acids were obtained from Sigma. Gadomer-17 was synthesized and kindly provided by Schering AG, viscotoxin A3 isolated from mistletoe was provided by the Zeeck group. DNA and β-peptide oligomers were synthesized by the Diederichsen group. All molecules were dissolved in water (Merck, LiChrosolv) at near neutral pH value (added buffer) with concentrations between 10^{-4} and 10^{-5} M and used without further purification. If necessary (in the case of DNA) the acidity of the solution was increased by adding sulfuric acid. Before the measurement the solutions were filtered (Schleicher and Schuell, 0.45 μm) and degassed.

3. Results and discussion

3.1. Applications of liquid beam mass spectrometry to different types of biomolecules

In the present article we summarize experimental results for molecules that belong to different families of
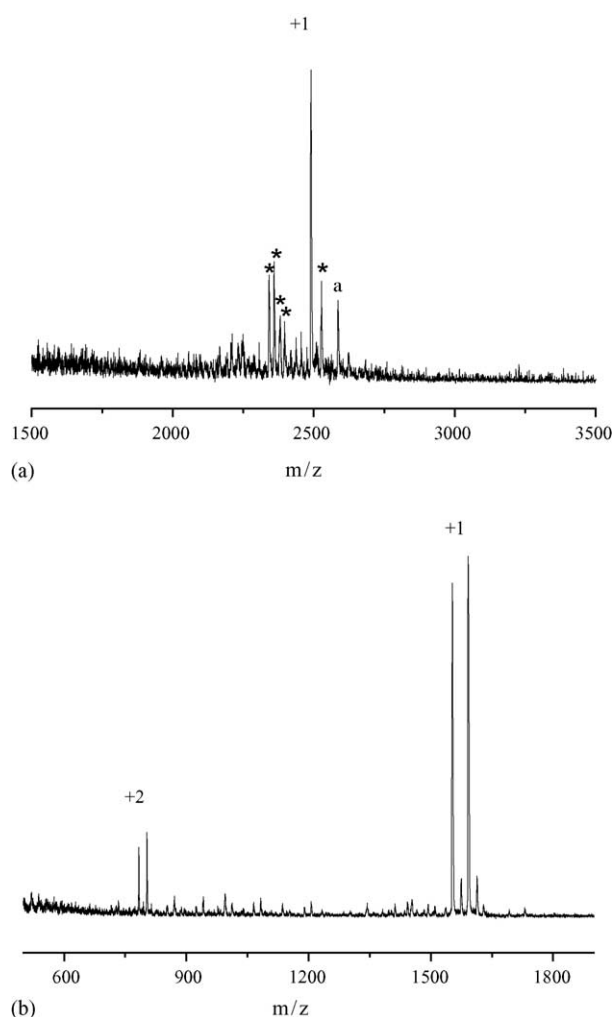
Fig. 2. (a) Mass spectrum of a DNA oligomer with the sequence 5′-GCCGCGGC-3′ ($C_{76}H_{98}N_{32}O_{49}P_8$, 2490 Da) at pH = 2. $E_{IR} = 0.7$ mJ/pulse at 2800 nm. Concentration: 5×10^{-5} M. The number on top of the peak labels the charge state (+2 not observed). The small lines marked with an asterisk around the parent mass peak of the DNA oligomer are peaks from protonated water clusters (spacing: 18 mass units), the single peak labelled by the letter 'a' has been attributed to a protonated sulfuric acid adduct (which had been added to set pH = 2). (b) Mass spectrum of two synthetic β-peptides (mixture) with nucleobases covalently attached to every third amino acid side chain in phosphate buffer (pH = 7) ($C_{73}H_{119}N_{25}O_{13}$ and $C_{74}H_{119}N_{27}O_{13}$ at 1553 and 1593 Da). $E_{IR} = 0.7$ mJ/pulse at 2735 nm. Concentrations: 3×10^{-5} M each. The number on top of the peak labels the charge state.

biomolecules in order to explore and extend the range of applications of the present technique. In Fig. 2a a mass spectrum is shown for a synthetic DNA oligomer. It is known that DNA is usually forming negatively charged adducts in water [11] solution which posed a problem for the present experiment which is designed to detect only positively charged aggregates. Decreasing the pH value to pH = 2, however, enabled us to monitor the DNA oligomer as a singly protonated species. Doubly charged double stranded DNAs are not stable under these conditions and therefore we do not expect doubly charged dimers at the mass position of the singly

charged monomer. This feature of the desorption techniques appears interesting because it enables the investigation of biomolecules present in their anionic form in solution in the positive ion detection mode of the experiment. In recent investigations Gupta et al. [20] have demonstrated that double-stranded DNA-drug complexes can also be observed with the electrospray technique in positive ion mode. For liquid beam desorption mass spectrometry it appears clear, however, that pH sensitive molecules or weakly bound aggregates of DNA may better be investigated in the negative mode [11].

A mass spectrum of two β-peptide decamers with nucleobases covalently linked to every third amino acid side chain is displayed in Fig. 2b [21]. Structurally in these synthetic oligomers a non-charged peptide backbone is combined with DNA nucleobases (Fig. 3a) as it is well known from peptide nucleic acids (PNA). On the other hand, these oligomers represent peptide secondary structures with the potential for non-covalent interactions [22]. Singly and doubly protonated adducts are formed and were easily detected in the positive ion mode at pH = 7 (buffered solution). The two close peaks in Fig. 2b correlate with the two oligomers that differ only in the nucleobase sequence (smaller peaks close to the parent mass peaks belong to water clusters). It is worth noting that beyond the fact that the two PNA oligomers (mixture) are desorbed softly the relative intensity of the mass peaks nicely reflects relative concentrations in solution.

Fig. 4a shows a mass spectrum of gadomer 17, a 17454 Da macromolecule bound to 24 gadolinium atoms which is a potential contrast medium in magnetic resonance tomography and neutron radiography. Due to the large number of basic groups in the molecule (see Fig. 3b) which are accessible to protonation the detection of the molecules did not pose any problems in positive ion mode of the mass spectrometer.

In Fig. 4b a spectrum of viscotoxin A3 is shown. Viscotoxins are toxic proteins isolated from *Viscum album* L. They are cystein rich basic microproteins (46 amino acids) with an approximate molar mass of 5 kDa. Several isoforms are known to date which have been shown to have both immunomodulating and cytotoxic properties, with the latter being interesting for complementary cancer therapy. Viscotoxin A3 was isolated from mistletoe (*Viscum album* L.). Its structure in solution has been characterized via NMR spectroscopy [23] and X-ray diffraction [24]. As cytochrome *c* the viscotoxin A3 contains many basic amino acids that are easily protonated in the experiment and enable an easy detection of the singly and doubly protonated species in positive ion mode of the spectrometer. In future experiments the membrane activity of this molecule in membrane models may be studied via mass spectrometry based methods.

Although, the mass resolution obtained is still somewhat limited the present approach appears to be an interesting alternative to other established techniques to desorb low charge molecular aggregates directly from their natural environment (i.e., water) and to measure biomolecule concentrations in solution quantitatively, a topic that is discussed in detail in the following section.

3.2. Quantitative detection of biomolecules in solution via laser induced liquid beam desorption mass spectrometry

An important issue for the analysis of biomolecules with mass spectroscopy is to make quantitative measurements of the biomolecules in solution. While the sensitivity of modern mass spectrometers employing ESI and MALDI is quite impressive, quantitative measurements of biomolecular concentrations is still a major issue. The non-linearity or the semi-quantitative behavior mainly stems from the soft desorption technique. It is well known that MALDI-MS is a beautiful technique but it is intrinsically non-linear and its limitations in the quantization are likely due to the still poorly characterized desorption process and the detour via an artificial matrix. Also ESI-MS is not without problems if quantitative measurements are required. The relationship between signal intensity and original analyte solution concentration has been studied extensively [25–28]. A typical relation between ESI-MS response and concentration is characterized by two distinct regions. The first region, often referred to as the linear dynamic range, represents a concentration range from the lower limit of detection up to about 10^{-5} M, where the signal response increases linearly with increasing concentration. In a second region encompassing progressively higher concentrations, the signal intensity levels off and may finally even decrease as concentration is further raised [29]. A further complication is that the increase in the linear range, and the concentration where transition into the "level off" region occurs, are different for ions of different charge state.

Often "molecular standards" circumvent the problem that a technique is not linearly responding to different concentrations in solution. This problem is particularly severe if concentrations in the solution phase are actually changing and if mass spectrometry is chosen to be the technique to measure these changes. Therefore, there is a large demand for quantitative biomolecule analysis beyond the powerful and well established MALDI and ESI-MS techniques. One technique that is relatively new as opposed to the latter ones is laser induced liquid water beam desorption mass spectrometry. Nevertheless, it has not been demonstrated hitherto that the technique can monitor solution concentrations linearly and in a quantitative way. A special aspect of the present study was the question whether liquid beam desorption and subsequent mass spectrometry in the gas phase provides a quantitative tool for measuring concentrations of biomolecules in solution. In Fig. 5 the concentration dependence of the gas phase mass peak (MH$^+$) for bovine serum albumin (∼66 kDa) in 10 mM ammonium acetate buffer between 10^{-3} and 10^{-6} mol/l is displayed. In the insert of Fig. 5 a mass spectrum for 10^{-4} M solution of BSA in water (with 10 mM NH$_4$Ac buffer) solution is shown. Quite impressively, we found that the gas phase signal of singly protonated BSA from water solution is linear over a concentration range of at least three orders of magnitude making the technique a promising quantitative tool for online monitoring of

(a)

(b)
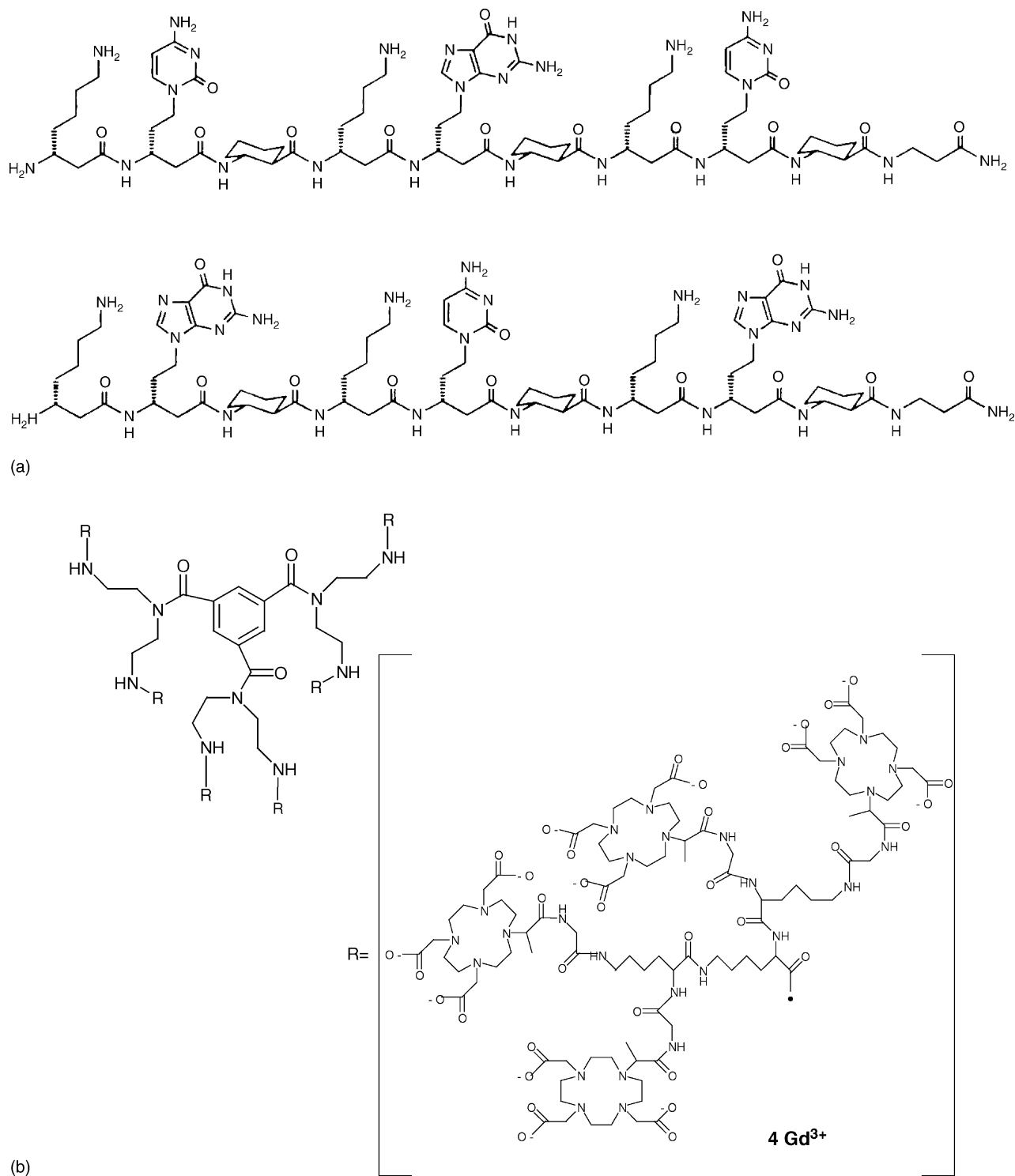
Fig. 3. (a) Structure of two synthetic β-peptide oligomers ($C_{73}H_{119}N_{25}O_{13}$ and $C_{74}H_{119}N_{27}O_{13}$) of mass 1553 and 1593 Da. (b) Structure of 24Gd[gly-medota]-trismesin-acid-hexa(trilys)-kaska-polymer abbreviated gadomer 17 ($C_{585}H_{927}Gd_{24}N_{165}O_{213}$, 17454 Da).

biomolecules in solution. This feature is not unique for BSA but has also been observed for many other molecules. Time resolved studies of changing concentrations in solution would enable to measure true rate constants of processes involving biomolecules in solution.

3.3. Mechanism and salt concentration dependence of liquid beam desorption

A complete treatment of all mechanistic aspects of liquid beam desorption with an infrared laser is certainly beyond
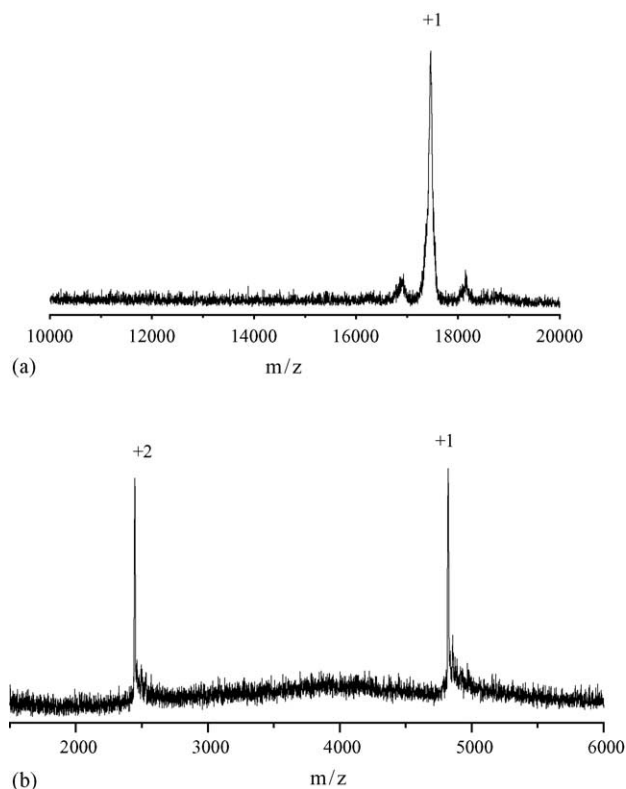
Fig. 4. (a) Mass spectrum of singly protonated (MH$^+$) gadomer 17 (C$_{585}$H$_{927}$Gd$_{24}$N$_{165}$O$_{213}$, 17454 Da). E_{IR} = 0.6 mJ/pulse at 2800 nm. Concentration: 3×10^{-5} M. pH = 7. (b) Mass spectrum and charge states (M + 2H$^+$ and MH$^+$) of viscotoxin A3 (C$_{201}$H$_{328}$N$_{62}$O$_{64}$S$_6$, 4829 Da). E_{IR} = 0.6 mJ/pulse at 2800 nm. Concentration: 3×10^{-5} M. pH = 7.

the scope of the present article. However, the main ideas and a few mechanistic features will be highlighted here in order to rationalize the observed mass spectra. One may anticipate from the very different approach that the condensed phase-to-
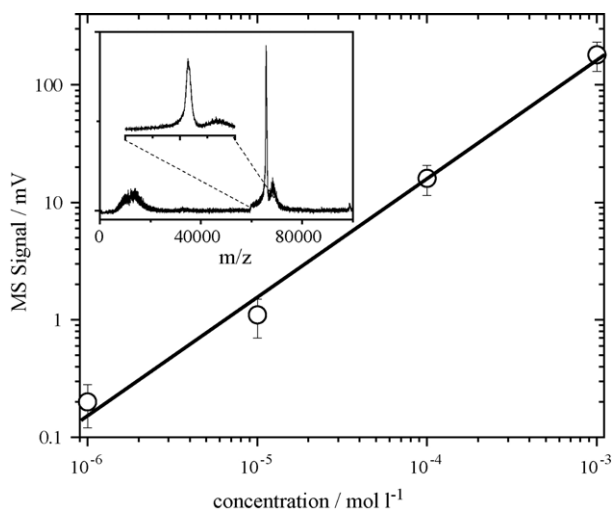
Fig. 5. Concentration dependence of the gas phase mass peak (MH$^+$) for bovine serum albumin (∼66 kDa) in ammonium acetate buffer between 10^{-3} and 10^{-6} mol/l (M). In the insert the mass spectrum for 10^{-4} M solution of BSA in water (with 10 mM NH$_4$Ac buffer) solution is displayed.

vacuum transfer of molecules and the "ionization process" in the case of liquid beam laser desorption is different from ion generation in the electrospray and the solid matrix desorption technique. Although, a direct ion evaporation from the liquid phase can be ruled out due to the large solvation energy, it is not clear, however, how the molecules are isolated and ejected at all from a hot water filament without destruction, as well as how and where are they charged, which is a prerequisite for mass spectrometric analysis.

As in the MALDI process we use laser absorption in a (liquid water) matrix to convert laser light energy into heat and to eject molecules and molecular aggregates from the (disintegrating) matrix. Depending upon the homogeneity and characteristics of laser photon energy deposition (being a function of laser energy, intensity, pulse length, and wavelength) in the liquid filament we may distinguish three cases: (i) supercritical gas expansion (case A), (ii) explosive thermal (spinodal) decomposition (case B), and (iii) shock wave dispersion (case C). In the following we will provide evidence and support for our hypothesis that the present experimental results are mostly consistent with a case B/C scenario and competition between these two cases.

Coming back to the question how the molecules are ejected and charged it is simple to show that the energy input is sufficient to completely evaporate the water jet. If we assume that for a 0.5 mJ pulse about 1/5 of the energy strikes the water filament we have about 0.1 mJ for the desorption which is 10 times larger than required for complete evaporation of the irradiated water volume. In principle, the energy input could be sufficient to physically disrupt the beam and eject superheated droplets or hot gas with biomolecules or both either in an ordinary spinodal decomposition or via a supercritical phase expansion. The mechanism and origin of the final charging of the biomolecules is also crutial but nevertheless not well understood. Brutschy and co-workers [9–11] and we [13,14] have argued recently that under certain circumstances the heating of the volume to a supercritical phase may be followed by an explosive expansion of the laser heated volume, which accelerates solvent as well as solute molecules. During the expansion the density and the dielectricity constant of the water environment decreases and *preformed* ions/aggregates are "isolated". However, due to the reduced shielding of the ions anions and cations recombine to a large extent such that only a small fraction of ions can be detected in the experiments. Brutschy has termed this small fraction the "lucky survivors" of the thermal supercritical phase expansion. If on laser impact the microfilament is disrupted and dispersed into hot droplets that contain charges, these droplets may evaporate and pass the charge to the embedded biomolecule. It is known from the spray techniques that even without large electric fields droplets can be charged [30,31], so that evaporating droplets can concentrate proton charges onto the biomolecules they contain. Interestingly, Faubel et al. have shown that a fast flowing microwater filament can be charged to some extent depending upon the pH value of the solution which was explained with a non-equilibrium electrochemi-

cal diffusion current model (electrokinetic charging) [32]. In contrast, spinodal decomposition nominally should produce biomolecules in their ground state (i.e. uncharged) but that could subsequently pick up one or two charges from gas phase proton transfer processes. It should be noted, however, that recent LILBID experiment under solute competition conditions in Brutschy's group and our own experiments do not show a pronounced correlation of the MS signals with gas phase proton affinities of the solutes.

The scenario of a homogeneous supercritical phase implies that the heat exposure can easily give rise to fragmentation which is hardly observed. Also from high speed pictures of the desorption process (such as displayed in Fig. 1) a more or less isotropic (depending upon the wavelength and the penetration depth of the laser) expansion of a mixture of hot gas and droplets of various sizes as well as recondensing gas phase rather than an expansion of a homogeneous (supercritical) phase is supported. As we will show later, also the associated velocity distribution of desorbed clusters does not support the picture of a simple expansion of an enthalpy limited seeded beam.

The evaporation of charged droplets that pass their charge to the embedded biomolecules may be attractive at first glance. However, a simple estimation shows that heated water droplets cannot evaporate easily in vacuum – i.e. without an additional source of heat. The heat of evaporation of water is $\sim$40 kJ/mol (0.4 eV/molecule). For evaporation of an isolated droplet in vacuum that is still liquid the evaporation energy can only come from the internal energy of the droplet. The result is that evaporative cooling is very efficient. A simple estimate shows that the initial droplet temperature needs to be over 1000 K for complete evaporation. However, a droplet at this temperature would probably only exist on a very short timescale. Thus it unlikely that a larger hot liquid droplet is formed that evaporates completely in vacuum. This situation is certainly different from that for spray techniques where continuous evaporation takes place due to heating from a bath gas at high pressures.

Our favored picture of the process – which is supported to a large extent by experiment – can be summarized as follows: the absorption of IR laser light does not heat the irradiated volume homogeneously. This may be due to absorption along the beam, insufficient penetration depth or hot spots in the laser intensity profile. Under our experimental conditions the energy deposition is such that a strong shock wave is generated that disperses part of the microwater filament (non-thermal "desorption") [33,34]. This process is followed by an explosive *thermal* volume expansion [35]. The dispersion is in general so strong that the molecules are nearly desolvated, or embedded in very small nano-droplets on the order of a few nanometers, i.e., close to the spatial dimension of the biomolecules. The microsolvated molecules may be desorbed with a significant number of water molecules directly bound to surface residues, with a first solvation shell, or they may be in a nano-droplet/water aggregate with a size close to the size of the protein. The role of clusters in MALDI has

recently been reviewed by Karas and Kruegr [36] While the velocities of desorbed molecules in the second fraction are expected to be close to the enthalpy limited velocity of a hot seeded molecular beam the velocities of the first fraction can be much higher. From simple density arguments and features of shock wave desorption we anticipate that the molecular velocities, the aggregate size and the temperature of the ejected water aggregates (nano-droplets/aggregates) is likely different for different fractions.

In the present case the charge of biomolecules is due to protonation if no other cations in large concentrations are present in solution (e.g., Na$^+$). If the pH is decreased, e.g., by adding acid, the detectable "ion yield" in the gas phase increases until saturation. Normally, measurements are made in buffered solution at around pH = 7. The ionization now is assumed to depend upon the probability of finding a protonated species (water or biomolecule) in a certain (dispersed and isolated) volume that depends upon its concentration and upon the distribution of counter ions in solution. The probability per unit volume of finding an ion i at the origin and, simultaneously, an ion of species j at the point R_{ij} is [37]

$$\frac{N_i}{V} \frac{N_j}{V} \exp\left(-\frac{\omega_{ij}}{k_B T}\right), \qquad (1)$$

where ω_{ij} is the potential of mean force acting between ions i and j. While the short-range repulsive part of ω_{ij} can be approximated as a hard-sphere potential the long range interaction is the Coulomb potential $\Phi_i(R_j)$ that satisfies the *Poisson* equation [37]. The charge density around an ion (with radius a) results from the distribution of counter ions (charges) in the medium,

$$q_i(R) = \sum_\alpha e Z_\alpha \frac{N_\alpha}{V} \exp\left[-\frac{e Z_\alpha \Phi_i}{k_B T}\right] \qquad (R > a). \qquad (2)$$

The totality of all shells surrounding the cation at the origin must carry a negative charge just equal to the positive charge of the ion,

$$\int_a^\infty 4\pi R^2 q_i(R)\, dR = -Z_i e. \qquad (3)$$

Combination of Eq. (2) and the Poisson equation leads to the Poisson–Boltzmann equation that enables us to determine the potential Φ_i [37],

$$\Phi_i = \frac{Z_i e}{4\pi \varepsilon_0 D} \frac{e^{\kappa a}}{1 + \kappa a} \frac{e^{-\kappa R}}{R}, \qquad (4)$$

with D being the dielectricity constant and

$$\kappa = \sqrt{\frac{e^2}{\varepsilon_0 D k_B T} \sum_\alpha Z_\alpha^2 \frac{N_\alpha}{V}}. \qquad (5)$$

κ^{-1} is in turn identified as the Debye screening length l_D. It can be regarded to be a measure of the decay of the "ion cloud" around the central ion i. It is important to realize that l_D is proportional to the square root of the total ion concentration.

The point now is that if we disperse the liquid into droplets or spheres that are smaller than the Debye screening radius there is a good chance to obtain charged sphere or aggregates (microsolvated molecules). At the same time the probability of having two charges in the sphere is much smaller. The latter appears to be closely linked to the appearance of (low) charge states in the experiment. If the ion concentration becomes larger (addition of salt), the Debye screening length is decreasing. For a constant dispersion (droplet size) the probability of obtaining a net charge on the dispersed/isolated aggregates is decreasing for decreasing l_D according to Eqs. (2)–(5).

Although, other mechanisms of charging droplets and microbeams exist we propose the above to be mainly responsible for the "ionization process" in liquid microbeam desorption.

Electrokinetic charging of the fast flowing beam can be controlled by the pH value of the liquid water and displays a sigh reversal at pH = 7. Since biomolecules can be desorbed efficiently at pH-values smaller or higher than 7 as cationic or anionic adducts we conclude that such charging effect is not dominant for the desorption process of charged species. For sprays it is known that droplets may be generated with many charges. Charging of liquid droplets has been explained by the Lenard spray electrification mechanism [38], as arising from the electrical double layer of a liquid surface. Randomly charged droplets (2–50 μm) of both polarities are found to follow a Gaussian distribution with the average charge zero and a mean square charge q_{av}^2 proportional to droplet volume [39]. Leontovich applied the theory of fluctuations to the free energy of electrolytic solutions [40] and Natanson applied the Boltzmann probability to the energy of formation of a charged spherical region within an electrolytic solution in the presence of thermal motions [41]. They obtained a net neutral Gaussian charge probability with $q_{av} \propto \sqrt{c}$ assuming that a spray process does not alter the charge distribution [39]. However, the predictions from these approaches do not appear to be consistent with the experimental observations (see Sections 3.2 and 3.3).

In order to provide evidence on the mechanistic features of the liquid beam laser desorption process we summarize a few experimental observations below.

Cytochrome c is an electron-transporting protein with a heme prostetic group bound to cystein 14 and 17. In the present experiments 10^{-5} M cytochrome c (12500 Da) was desorbed from different solutions in order to study the features of the desorption process and the dependence of the efficiency of the process at different ion concentrations (added salt or buffer). In Figs. 6 and 7 we have given an overview of different experiments with different delay times (see Fig. 1b), i.e., times of the trigger of the ion optics relative to the desorption laser pulse, in which we probe the velocity distribution of desorbed species schematically depicted in Fig. 1b. While Fig. 6 summarizes experiments for 0.5 mJ/pulse Fig. 7 displays results for 0.7 mJ/pulse for similar focusing conditions. Depending upon the laser energy in the experiment and the desorption process cytochrome c is observed first be-
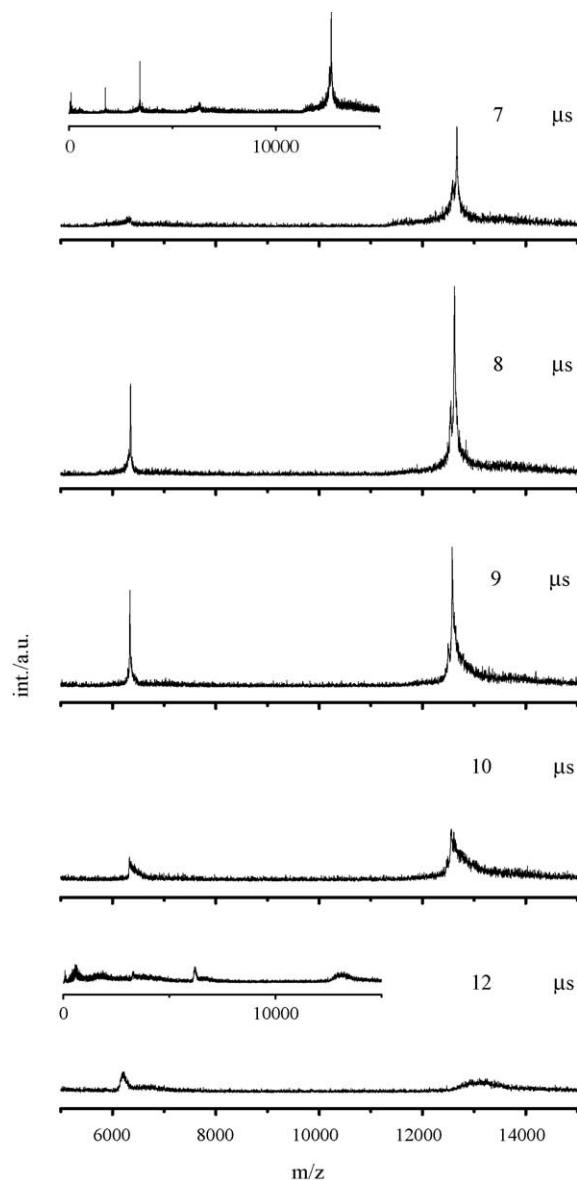
Fig. 6. Sequence of desorption experiments for cytochrome c in water solution with different delay times Δt for 0.5 mJ/pulse (λ_{IR} = 2800 nm) desorption energy. Note: the protonated cytochrome c is not fragmented at any time. Spectra show two prominent peaks, namely singly and doubly protonated cytochrome c at m/z = 12500 and 6250 Da, respectively (the doublet structure of the parent stems from small impurities rather than adduct formation or fragmentation).

tween 5 and 7 μs. The larger the absorbed energy (desorption laser pulse energy) the earlier the first fraction is observed in the experiment (note that a time delay of the ion optics of 5 and 12 μs corresponds to a molecular velocities of 6500 and 3500 m/s). The corresponding molecular velocities suggest that the first fraction of molecules is ejected by a strong shock wave desorption. These high velocities are well above the predictions for enthalpy limited hot gas expansions. Nevertheless, the later phase of the ejection we attribute to a thermal explosive decomposition and expansion (as apposed to the first non-thermal process).
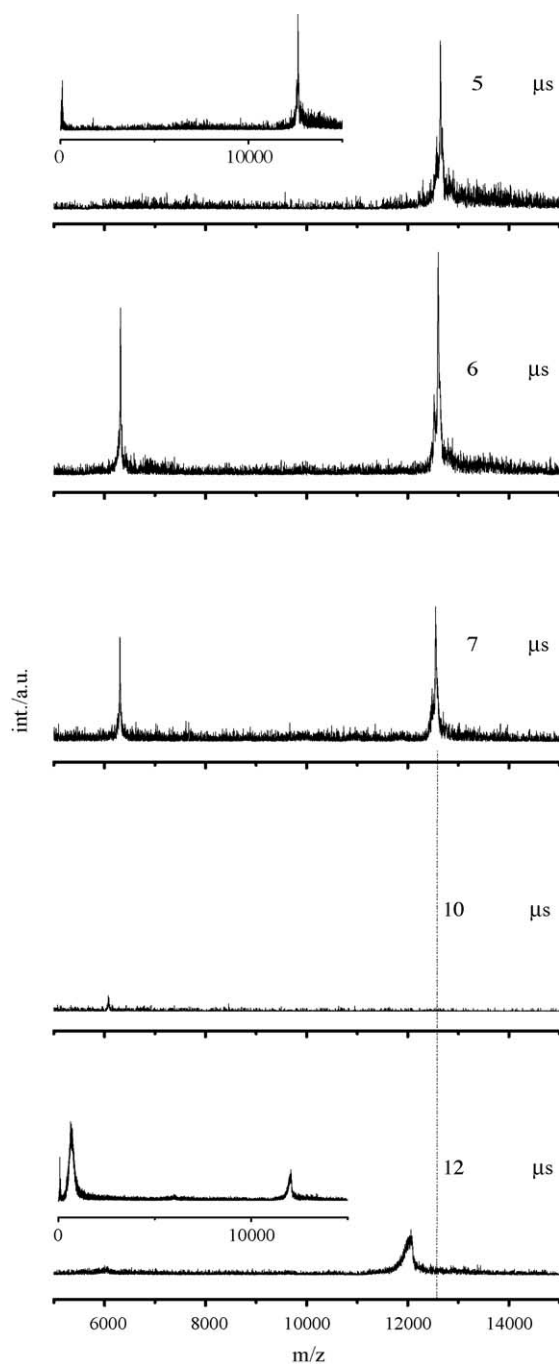
Fig. 7. Sequence of desorption experiments for cytochrome *c* in water solution with different delay times Δt as in Fig. 3 but for 0.7 mJ/pulse ($\lambda_{IR} = 2800$ nm) desorption energy. Note: the protonated cytochrome *c* has lost its heme group at long delay times (12 μs).

While in the first fraction only the singly protonated species are observed, at later times also higher charge states are visible. After 12 μs delay time the signal vanishes. It is worth noting that for 0.5 mJ pulse energy the cytochrome *c* protein is not fragmented at any time whereas for 0.7 mJ the heme group is lost at longer times (12 μs delay time). Both observations appear to be consistent with our conjecture that in the first phase of the desorption/dispersion nearly desol-

vated molecules or molecules with a thin solvent layer at not too high temperatures are desorbed. From the experiments we conclude that the water content ("droplet size") and the temperature increase for increasing delay (see Figs. 7 and 8)
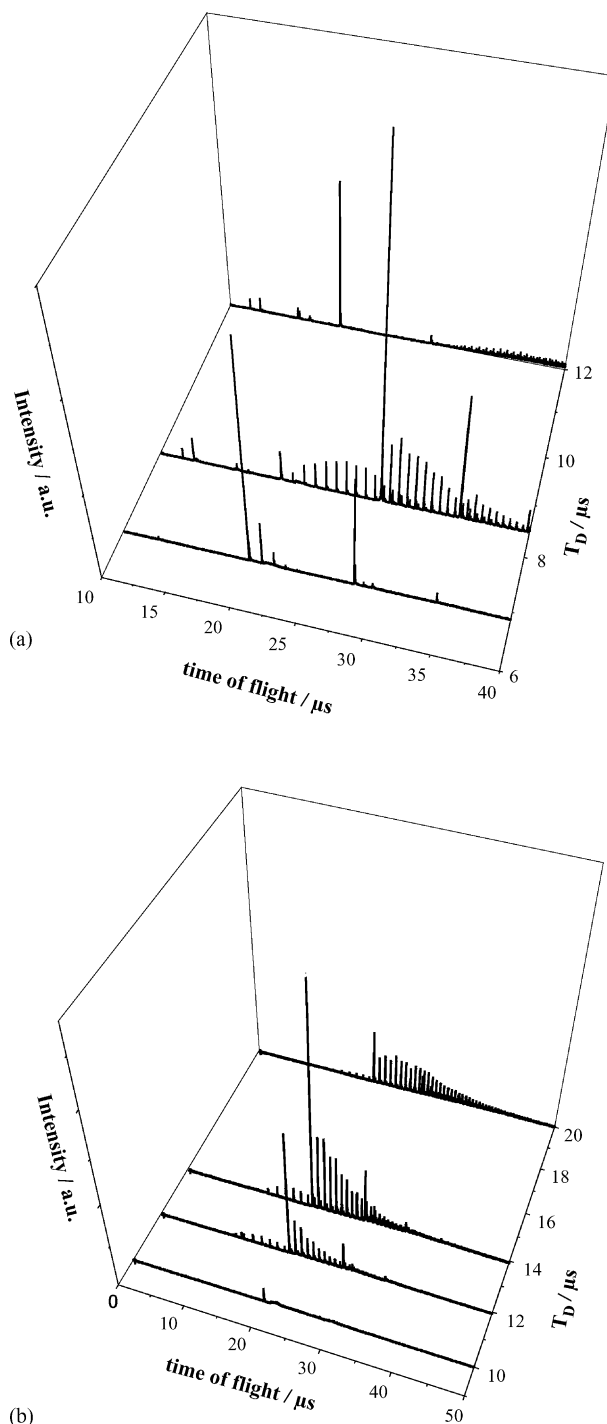
Fig. 8. (a) Time-of-flight (TOF) spectra of arginine ($0.01 \, mol \, l^{-1}$) as a function of delay time T_D for a higher desorption energy (0.75 mJ); (b) time dependent time-of-flight (TOF) spectra of arginine as in (a) for a lower desorption energy (0.5 mJ). Note: for these experiments the time-of-flight scale is mot converted into a mass scale. While the peak at 19 μs corresponds to the protonated amino acid parent the peak at 27 μs correlates with the singly protonated dimer.

which may be characteristic for fast non-thermal shock ejection and a subsequent thermal explosive decomposition. At early time the probability of finding two charges in the sphere (biomolecule with a more or less pronounced water layer) is low but increases with the size of the sphere (droplet). This may explain the features of the charge states in the present experiments. In addition in high temperature water at high densities the ion product of water is much larger than at ambient temperature [42,43]. The presence of excess hydronium ions (H_3O^+) under these conditions may strongly enhance protonation of basic sites of the solvated molecules and in turn their detection in the form of ionic aggregates.

For the larger desorption energy we find that at later times the high temperature of the larger nano-droplets causes a heme-group fragmentation consistent with the assumption that the aggregates are larger and hotter at later times and have the temperature as well as time to boil off the water completely. It is interesting to observe that for the lower desorption energy the molecules are not fully desolvated as can be seen from the asymmetric mass peaks. This asymmetry increases for increasing delay time which is consistent with the picture that the droplets at later times are larger and the temperature is in this experiment not high enough to fully desolvate the biomolecules for reasons we have explained above.

In order to test the mechanistic concept we have desorbed a much smaller molecule, i.e., arginine in water solution (0.01 mol l^{-1}). In Fig. 8 arginine time-of-flight spectra are displayed for two desorption conditions, namely 0.5 and 0.75 mJ. While the peak at 19 µs corresponds to the protonated amino acid parent the peak at 27 µs correlates with the singly protonated dimer. Even higher multimers are seen for the present high concentrations. For the present case the water clusters can be resolved easily. Interestingly, for the higher desorption energy (Fig. 8a) we observe desolvated protonated arginine and the singly protonated arginine dimer. The relative abundance of monomers and multimers very likely does not reflect their equilibrium concentration in solution but is a consequence of the overall high concentration and the probability of finding two molecules in the dispersed volume (nano-droplet). Consistent with the experiments on cytochrome *c* in the higher energy desorption a first fraction of molecules with high desorption velocities (6500 m s^{-1}) an intermediate fraction and a fraction with a velocity of 2500 m s^{-1} can be observed. While the first and fast fraction is completely desolvated the intermediate is not. Here, we observe large water clusters and even higher multimers. In the final fraction the molecules are again completely desolvated and the abundance of multimers is deceased again. This signature is nicely consistent with the cytochrome *c* data and our picture that for early times the molecules are desorbed via shock wave desorption with high velocities as nearly desolvated molecules or not too hot small water aggregates. For the intermediate fraction the droplet size but not the temperature is likely increased resulting in incomplete desolvation and a higher abundance of multimers. The shock desorption

is followed by a thermal (spinodal) decomposition that releases larger droplets with a higher temperature. For the final fraction the temperature appears to be so high that complete desolvation and dissociation of multimers occurs. This picture is further supported by similar experiments in Fig. 8b. In this case the early fraction due to shock wave desorption is missing and the slower thermal desorption possibly releases larger hot droplets (2500–3000 m s^{-1}) that can, however, not completely boil off the water during their flight time. Also in this case the pattern of the water clusters indicates larger nano-droplets for increasing delay time.

In another type of experiment we have added NaCl and ammonium acetate (acting as a buffer) to the water solution. In Fig. 9a) the dependence of the signal of the singly and doubly protonated cytochrome *c* on NaCl concentration is displayed. If salt, beyond 1 mM up to 100 mM is added a

(a)

(b)
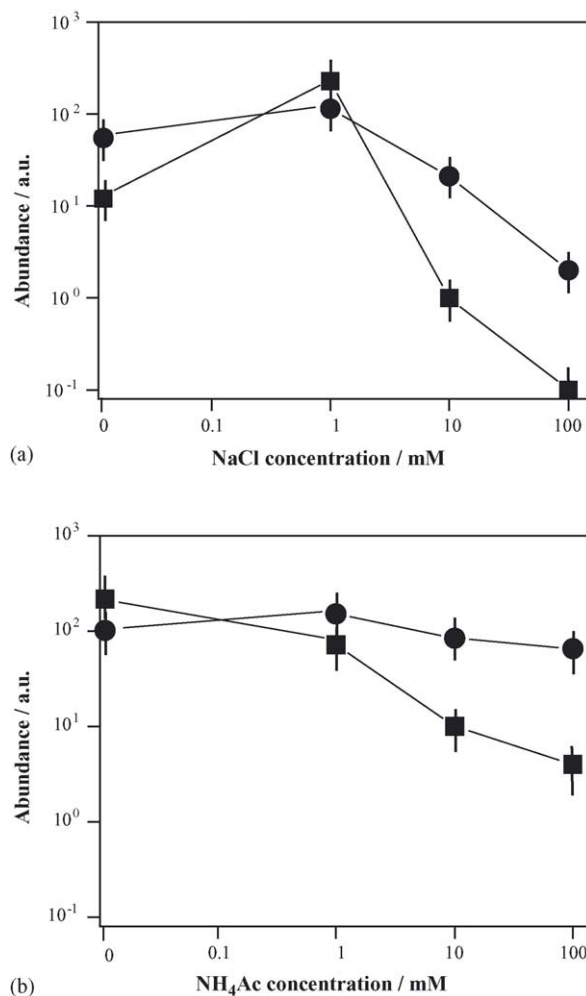
Fig. 9. (a) Mass peak intensities (abundance) for singly (filled circles) and doubly charged (filled squares) cytochrome *c* in water for different NaCl concentrations at $\Delta t = 7.5$ µs and for 0.5 mJ/pulse ($\lambda_{IR} = 2800$ nm). For concentrations less or equal to 10 mM the ratio of H$^+$ to Na$^+$ adducts is larger than 10 and approaching ≈ 1 at 100 mM. (b) Mass peak intensities (abundance) for singly and doubly protonated cytochrome *c* in water for different ammonium acetate concentrations at $\Delta t = 7.5$ µs and for 0.7 mJ/pulse ($\lambda_{IR} = 2800$ nm).

strong decrease of the overall signal is observed in qualitative agreement with Eqs. (2)–(5). Interestingly, the decrease for the higher charge states is more pronounced than for the singly charged aggregates, which is also consistent with Eqs. (2)–(5), implying that it is possible to shift the charge state distribution by adding electrolyte to the solution. Such an effect is also well known for the electrospray process [44]. From an analytical point of view [45] it is important to note that even for physiological solutions whose concentration is close to the highest concentrations investigated in this study biomolecules can be desorbed from the solution and analyzed without special preparation of the solution (removing salt).

For pH-sensitive biomolecules the pH value has to be stabilized with an added buffer. In a separate series of experiments we have investigated whether added buffer modifies the desorption process and in turn the mass spectra. In Fig. 9b we have displayed experiments in which ammonium acetate (NH_4Ac) is added to the solution. As in Fig. 4a we display the intensities of the mass peak for the singly and doubly charged cytochrome c as a function of NH_4Ac concentration. In this case the delay time of the experiment is similar to that in Fig. 4a. As in the previous case the addition of the ammonium acetate decreases the intensity of both charge states, however, the doubly charged species is much more affected (reduced). As is visible in Fig. 9b mass spectra can be recorded even much beyond the 100 mM concentration of ammonium acetate, a feature that is important for general biomolecule mass analysis.

4. Summary and conclusions

In summary, we have highlighted several applications of liquid beam desorption mass spectrometry for the analysis of biomolecules. In particular, cytochrome c, viscotoxin A3, synthetic DNA oligomers and nucleobase substituted β-peptides, bovine serum albumin, as well as specifically designed macromolecules for special pharmaceutical applications have been desorbed from water solution and analyzed with time-of-flight mass spectrometry. For the desorption of cytochrome c the tolerance of salt and buffer concentration has been measured. A special aspect of the present study was the question whether liquid beam desorption and subsequent mass spectrometry in the gas phase provides a quantitative tool for measuring concentrations of biomolecules (even in mixtures) in solution. With BSA as an example we have demonstrated that the gas phase signal of singly protonated BSA from water solution is linear over a concentration range of at least three orders of magnitude making the approach a promising quantitative tool for time resolved monitoring of biomolecule concentrations in solution.

Beyond the demonstration of several applications of this technique, mechanistic aspects such as the nature of the desorption process are addressed. With a field-free-drift time-of-flight approach we were able to monitor features of the desorption process by selecting fractions of the broad velocity distribution of desorbed species using an ion optics acting as an ion gate. The observed molecular velocities of desorbed protonated species and aggregates provide firm evidence for an interplay of an explosive thermal and a shock wave dispersion of the microfilament controlling the ejection of hot nano-droplets and microsolvated molecules. Charging and charge states of the biomolecules appear to be correlated with the Debye screening length of electrolytic solutions. Future molecular dynamics calculations similar to those of the Garrison group may shed more light into the intriguing laser induced desorption/dispersion process associated with microwater beams in vacuum [46,47]. A further interesting aspect is whether the present experimental results are relevant for pulsed laser ablation of tissues which contain between 60 and 90% liquid water [48].

The general goal in biomolecule mass spectrometry is to produce a gas-phase molecule that is completely desolvated implying that solvent disruption and molecule ejection is not enough but also the molecule must be heated sufficiently to boil off any residual solvent from its surface. This process may be important for cooling and stabilization of the biomolecule. Heating the molecule sufficiently to desolvate it on a short timescale without fragmentation is a delicate balance that appears possible with the present method. In the field-free drift region the molecules have several microseconds for the desolvation. This is a quite long time, such that the biomolecules need not to be exceptionally hot. This situation is different for MALDI with direct extraction. There, the biomolecule must desolvate in nanoseconds and therefore must be much hotter which in turn may result in more fragmentation.

Acknowledgments

References

[1] J.B. Fenn, M. Mann, C.-K. Meng, S.-F. Wong, G.M. Whitehouse, Science 246 (1989) 64.
[2] T. Tanaka, M. Waki, Y. Ido, Y. Akita, Y. Yoshida, T. Yoshida, Rap. Comm. Mass Spectrom. 2 (1988) 151.
[3] J. Wei, J.M. Buriak, G. Siuzdak, Nature 399 (1999) 243.
[4] M. Karas, F. Hillenkamp, Anal. Chem. 60 (1988) 2299.
[5] F. Sobott, W. Kleinekofort, B. Brutschy, Anal. Chem. 69 (1997) 3587.
[6] F. Sobott, A. Wattenberg, H.-D. Barth, B. Brutschy, Int. J. Mass Spectrom. 185–187 (1999) 271.

[7] A. Wattenberg, H.-D. Barth, B. Brutschy, J. Mass Spectrom. 32 (1997) 1350.

[8] A. Wattenberg, F. Sobott, H.-D. Barth, B. Brutschy, Int. J. Mass Spectrom. 203 (2000) 49.

[9] W. Kleinekofort, A.J.B. Brutschy, Int. J. Mass Spectrom. Ion Proc. 152 (1996) 135.

[10] W. Kleinekofort, A. Pfenninger, T. Plomer, C. Griesinger, B. Brutschy, Int. J. Mass Sectrom. Ion Proc. 156 (1996) 195.

[11] W. Kleinekofort, M. Schweitzer, J.W. Engels, B. Brutschy, Int. J. Mass Spectrom. Ion Proc. 163 (1997) 1L.

[12] M. Faubel, T. Kisters, Nature 339 (1989) 527.

[13] A. Charvat, E. Lugovoj, M. Faubel, B. Abel, Eur. Phys. J. D 20 (2002) 573.

[14] A. Charvat, E. Lugovoj, M. Faubel, B. Abel, Rev. Sci. Instr. 75 (2004) 1209.

[15] B. Stasicki, A. Charvat, M. Faubel, B. Abel, SPIE Proceedings of the 26th International Congress on High Speed Photography and Photonics, vol. 5580, 2005, p. 72.

[16] N. Hirimoto, J. Kohno, F. Mafune, T. Kondow, J. Phys. Chem. A 103 (1999) 9569.

[17] J. Kohno, F. Mafune, T. Kondow, Chem. Lett. 92 (2002) 562.

[18] S. Woutersen, U. Emmerichs, H.J. Bakker, Science 278 (1997) 658.

[19] H.-K. Nienhuis, S. Woutersen, R.A. Santen, H.J. Bakker, J. Chem. Phys. 111 (1999) 1494.

[20] R. Gupta, A. Kapur, J.L. Beck, M.M. Sheil, Rap. Comm. Mass Spectrom. 15 (2001) 2472.

[21] A.M. Brückner, M. Garcia, A. Marsh, S.H. Gellman, U. Diederichsen, Eur. J. Org. Chem. 10. (2003).

[22] A.M. Brückner, P. Chakraborty, S.H. Gellman, U. Diederichsen, Angew. Chem. Int. Ed. 42 (2003) 4395.

[23] S. Romagnolli, R. Ugolini, F. Fogolari, G. Schaller, K. Urech, M. Giannattasio, L. Ragona, H. Molinari, Biochem. J. 350 (2000) 569.

[24] J.E. Debreczeni, B. Girmann, A. Zeeck, R. Krätzner, G.M. Sheldrick, Acta Cryst. D59 (2003) 2125.

[25] R. Kostiainen, A.P. Bruins, Rap. Comm. Mass Spectrom. 8 (1994) 549.

[26] J.B. Fenn, J. Am. Soc. Mass Spectrom. 4 (1993) 524.

[27] P. Kebarle, L. Tang, Anal. Chem. 972A (1993).

[28] J. Sunner, G. Nicol, P. Kebarle, Anal. Chem. 60 (1988) 1300.

[29] P. Kebarle, J. Mass Spectrom. 35 (2000) 804.

[30] M. Ziaei-Moayyed, E. Goofman, P. Williams, J. Chem. Ed. 77 (2000) 1520.

[31] W.L. Holstein, L.J. Hayes, E.M.C. Robinson, G.S. Laurence, M.A. Buntine, J. Phys. Chem. B 103 (1999) 3035.

[32] M. Faubel, B. Steiner, Ber. Bunsenges. Phys. Chem. 96 (1992) 1167.

[33] P. Williams, R.W. Nelson, in: K.G. Standing, W. Ens (Eds.), Methods and Mechanisms for Producing Ions from Large Molecules, Plenum Press, New York, 1991, p. 265.

[34] R.E. Johnson, S. Banerjee, A. Hedin, D. Fenyö, B.U.R. Sundquist, Heavy Ion and Laser Pulse Induced Ejection of Large Organic Molecules, Plenum Press, New York, 1991.

[35] J. Hohno, F. Mafune, T. Kondow, Chem. Lett. 23 (2002) 562.

[36] M. Karas, R. Kruegr, Chem. Rev. 103 (2003) 427.

[37] H.L. Friedman, Ionic Solution Theory, Wiley, New York, 1962.

[38] P. Lenard, Ann. Phys. 47 (1915) 463.

[39] E.E. Dodd, J. Appl. Phys. 24 (1953) 73.

[40] M. Leontovich, Comp. Rend. Acad. Sci. URSS 53 (1946) 111.

[41] G.L. Natanson, Comp. Rend. Acad. Sci. URSS 53 (1946) 115.

[42] W.L. Marshall, E.U. Franck, J. Phys. Chem. Ref. Data 10 (1981) 295.

[43] K. Pitzer, J. Phys. Chem. 86 (1982) 4704.

[44] G. Wang, R.B. Cole, Electrospray Ionization Mass Spectrometry: Fundamentals, Instrumentation, and Applications, Wiley, New York, 1997.

[45] N. Mano, J. Goto, Anal. Sci. 19 (2003) 3.

[46] Y. Dou, N. Winograd, B.J. Garrison, L.V. Zhigilei, J. Phys. Chem. B 107 (2003) 2362.

[47] Y. Dou, L.V. Zhigilei, Z. Postawa, N. Winograd, B.J. Garrison, Nucl. Instr. Meth. Phys. Res. B 180 (2001) 105.

[48] A. Vogel, V. Venugopalan, Chem. Rev. 103 (2003) 577.